Miniature Viscous Disk Pump: Performance Variations From Non-Newtonian Elastic Turbulence

Phil Ligrani
Fellow ASME
Propulsion Research Center,
Department of Mechanical and
Aerospace Engineering,
University of Alabama in Huntsville,
5000 Technology Drive,
Olin B. King Technology Hall S236,
Huntsville, AL 35899
e-mail: pml0006@uah.edu

Benjamin Lund
Propulsion Research Center,
Department of Mechanical and
Aerospace Engineering,
University of Alabama in Huntsville,
5000 Technology Drive,
Olin B. King Technology Hall N202A,
Huntsville, AL 35899
e-mail: brl0007@uah.edu

Arshia Fatemi
Robert Bosch GmbH (CR/ARF2),
Robert Bosch Central Research 130-1,
Robert Bosch Campus 1,
Renningen 71272, Germany
e-mail: Arshia.Fatemi@de.bosch.com

Within the present investigation, a miniature viscous disk pump (VDP) is utilized to characterize and quantify non-Newtonian fluid elastic turbulence effects, relative to Newtonian flow behavior. Such deviations from Newtonian behavior are induced by adding polyacrylamide to purified water. The VDP consists of a 10.16 mm diameter disk that rotates above a C-shaped channel with inner and outer radii of 1.19 mm and 2.38 mm, respectively. A channel depth of 230 μm is employed. Fluid inlet and outlet ports are located at the ends of the C-shaped channel. Experimental data are given for rotational speeds of 126 1/s, 188 1/s, 262 1/s, and 366 1/s, pressure rises as high as 700 Pa, and flow rates up to approximately 0.00000005 m^3/s. Reynolds number ranges from 2.9 to 6.5 for the non-Newtonian polyacrylamide solution flows and from 51.6 to 149.8 for the Newtonian pure water flows. To characterize deviations due to non-Newtonian elastic turbulence phenomena, two new parameters are introduced, PrR and HCR, where HCR is the ratio of head coefficient (HC) for the polyacrylamide solution and head coefficient for the water solution, and PrR is the ratio of pump power for the polyacrylamide solution and pump power for the water solution. Relative to Newtonian, pure water flows, the polyacrylamide solution flows give pump head coefficient data, dimensional pressure rise data, slip coefficients (SCs), specific speed (SS) values, and dimensional power data, which show significant variations and differences as they vary with flow coefficient (FC) or dimensional volumetric flow rate. Also important are different ranges of specific speed (SS) for the pure water and polyacrylamide solutions, and a lower range of SC or slip coefficient values for the polyacrylamide solution flows, compared to the pure water flows. These variations are due to increased elastic turbulence losses, which occur as viscosity magnitudes increase and the elastic polymers are excited by mechanical stress, which causes them to extend, deform, stretch, and intertwine. [DOI: 10.1115/1.4034522]

Introduction

Of recent studies which consider the influences of non-Newtonian fluid flows on pump operation and performance, Yu et al. [1] investigated flow patterns, velocity distributions, and shear stress distributions in macroscale centrifugal pumps with four different impeller arrangements. Of particular interest are influences of blood flow on pump performance, as well as the effects of the pumps on blood characteristics, especially thrombus formation and hemolysis. The presence of recirculation vortices and recirculation regions is considered for all the four impeller configurations. Additional discussion of the effects of fluid viscosity on centrifugal pump performance is provided by Li [2]. Variations of pump head, efficiency, and power are provided over a range of volumetric flow rates for water and oil flows. According to this investigator, centrifugal pump performance decreases as fluid viscosity increases, because of increases of friction losses over the surfaces of the impeller shroud and hub, and because of larger hydraulic losses within the flow passages inside the impeller. Zhang et al. [3] investigated the operation and performance of a magnetically suspended impeller centrifugal blood pump, or ventricular assist device (VAD). Flows of water and an aqueous Xanthan gum solution are investigated, where the gum solution is utilized to model non-Newtonian blood flow. According to the investigators, this solution is a shear-thinning, drag-reducing fluid. Overall, pump head rise with the aqueous Xanthan gum solution is lower, relative to water flow at the same volumetric flow rate, when the pump operates at low rotor speeds. However, for higher rotor speeds, pump head magnitudes with the aqueous Xanthan gum solution are higher than for water flows, when compared at the same volumetric flow rates. Memardezfouli and Nourbakhsh [4] investigated slip factors in centrifugal pumps. Presented are the impeller exit slip factors as they vary with passage width for different FCs. Slip factor data are also presented over a range of FCs, for five different impeller arrangements, which are corrected for flow distortion at the impeller periphery.

Only a few studies are available which address variations due to non-Newtonian fluid flows on microscale or millimeter-scale pump performance. Of the relevant investigations, da Silva et al. [5] and El-Sadi et al. [6] described non-Newtonian flow behavior in micropumps. For the former study, optimization of devices for biomedical application is considered for configurations which are similar to the ones investigated by Sen et al. [7]. Berli [8] described the development of electrokinetic pumping of non-Newtonian fluids through cylindrical and slit microchannels. For some flow conditions, the microstructure of the non-Newtonian fluids is altered near solid–liquid interfaces. With this situation, output pressure and pumping efficiency are significantly higher than present with simple electrolyte solutions at the same experimental conditions. Ligrani et al. [9] considered deviations due to non-Newtonian influences within the same type of miniature VDP, which is employed within the present study. In that investigation, deviations from Newtonian behavior are induced by adding different concentrations of sucrose to purified water, with increasing non-Newtonian characteristics as sucrose concentration increases from 0% (pure water) to 10% by mass.

Contributed by the Fluids Engineering Division of ASME for publication in the Journal of Fluids Engineering. Manuscript received March 28, 2016; final manuscript received August 10, 2016; published online November 3, 2016. Assoc. Editor: Hui Hu.

 Copyright © 2017 by ASME

Downloaded From: http://fluidsengineering.asmedigitalcollection.asme.org/pdfaccess.ashx?url=/data/journals/jfega4/935857/ on 03/31/2017 Terms of Use: http://www.asme.org/a

The present investigation is unique because the performance of a miniature VDP [10,11] is considered with non-Newtonian elastic turbulence flow, relative to Newtonian water flow. Such behavior is induced using elastic polymer solutions within liquids as they are excited by a mechanical stress, which causes them to exhibit highly nonlinear and non-Newtonian behavior. The polymer additive employed in the present study is polyacrylamide. The extensibility of the polymer and the resulting polymer deformation lead to a sharp growth in the local elastic stress, a sequence of events referred to as the Weissenberg instability [12], which occurs when the Weissenberg number is greater than a threshold value which depends upon the flow conditions and configuration. When this occurs, elastic turbulence is present, which results in increased polymer viscosity, in some cases, by up to 3 orders of magnitude [12]. As such, the present investigation is unique and different from prior investigations since characterization and quantification of the effects of non-Newtonian elastic turbulence on miniature VDP performance are considered.

The miniature VDP is of millimeter-scale, with a channel depth of 230 μm. The VDP is utilized because it produces easily controlled flow rates and pressure rises, as simplicity and ease of manufacturing are maintained [9,10]. The disk pump is unique because it uses viscous stress to produce a pumping effect by employing one disk and a C-shaped channel [9,10]. As the fluid passage height becomes smaller, the Reynolds number decreases, and the viscous forces become more significant relative to inertial forces. To quantify deviations due to non-Newtonian elastic turbulence phenomena, variations of pump HC, flow coefficient, slip coefficient, specific speed, dimensional pressure rise, dimensional volumetric flow rate, and dimensional power are presented. Also provided is a new head coefficient ratio parameter, which represents the normalized pressure rise change at a particular flow rate and polyacrylamide concentration, as elastic turbulence phenomena are induced. The present experimental data are given for rotational speeds from 126 to 366 rad/s, pressure rises as high as 700 Pa, and flow rates up to approximately 0.00000005 m^3/s.

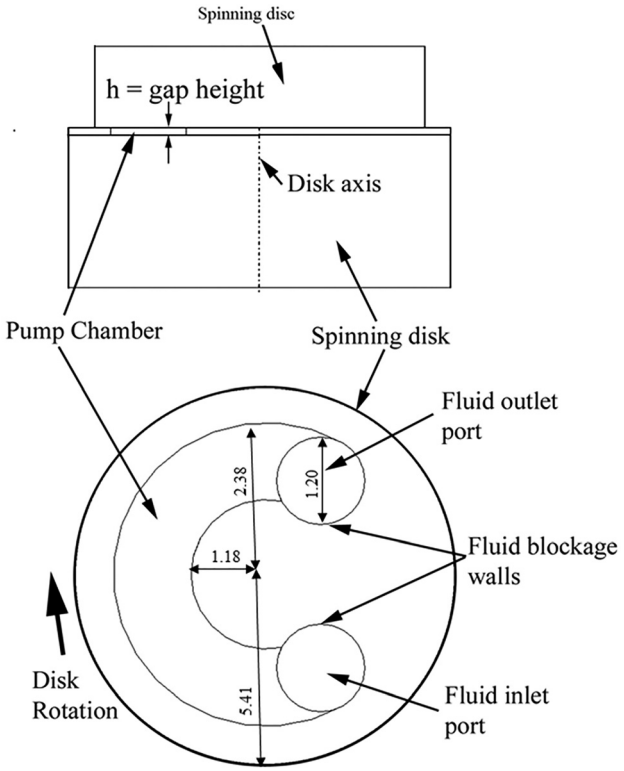

Fig. 1 Cross-sectional view and side view of the viscous disk pump—VDP. All the dimensions are given in millimeters.

Miniature Viscous Disk Pump Configuration and Operation

The pump consists of a spinning disk and a C-shaped channel with a fluid inlet port and a fluid outlet port, which are located at opposite ends of the C-shaped flow channel [9–11]. The overall arrangement is shown in Fig. 1, and the coordinate system is shown within Fig. 2. There are three main components of the pump: (i) the fluid chamber assembly, (ii) the disk and shaft, and (iii) the motor and pump housing. Details regarding these different items are provided by Ligrani et al. [9,11] and Blanchard et al. [10].

As shown in Fig. 1, as the disk rotates, its edges remain in contact with the fluid chamber walls, creating a seal that minimizes leakage of the test fluid from the fluid chamber. Rotating Couette-type flow is thus induced in the fluid chamber between the rotating disk and the stationary bottom of the channel. A circumferential pressure gradient is then present in the fluid chamber because of the work done on the fluid within the C-shaped channel by the rotating disk. The disk diameter is 10.16 mm. This interaction gives Poiseuille-type flow, with a static pressure rise with circumferential position through the pump chamber volume, such that a region of lower static pressure is present near the fluid inlet port, and a region of higher static pressure is present near the fluid outlet port. Pressure rise measurements are made across the pressure ports shown in Fig. 2.

Experimental Apparatus and Procedures

Figure 3 shows the experimental arrangement and components for the VDP. The disk pump is powered by an externally mounted Maxon EC32 #118890. The motor has a 48 V winding, a power rating of 80 W, a maximum speed of 25,000 rpm, and a stall torque of 0.353 Nm. The motor is controlled by a Maxon ESCON 50/5 #409510 motor controller connected to an Advanced Motion Controls model PS2X3W48 power supply. The power supply has a dc supply voltage of 48 V, a peak current of 12 A, and a continuous current rating of 6 A. The motor controller maintains a constant speed through a closed control loop and a Maxon HEDL 55 Encoder #110514. The speed and direction of the motor are controlled by regulating voltage to the analog and digital I/O channels

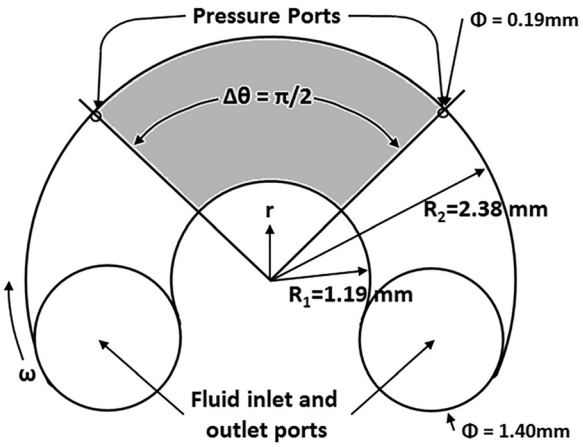

Fig. 2 Configuration of the single-disk viscous pump, including coordinate system. The shaded region of the pump chamber is used for the flow analysis. The *z*-coordinate is directed normal to the surface and measured from the halfway location between the surface and the disk, at the horizontal center plane of the flow passage.

Downloaded From: http://fluidsengineering.asmedigitalcollection.asme.org/pdfaccess.ashx?url=/data/journals/jfega4/935857/ on 03/31/2017 Terms of Use: http://www.asme.org/a

on the motor controller using LABVIEW 32-bit software, version 10.0.1, and a National Instruments USB-6003 data-acquisition card. The rotational speed measurement system is calibrated using a timing light.

A DP-15 Validyne differential pressure transducer is used to measure the differential pressure between the pressure ports. The transducer employs a number 20 diaphragm which can measure pressure differentials with ranges up to 872 Pa. The output signal from the pressure sensor is processed using a Celesco Model number CD15 Carrier Demodulator. This demodulator produces a voltage output that is read by a National Instruments USB-6210 data-acquisition board and LABVIEW 32-bit software, version 10.0.1. All the data are recorded, and then entered and processed using a Dell Precision T1700 computer workstation.

A Key Instruments model 1XLW9 flow meter is used to measure the time-averaged fluid flow rate. This device is used for measurements of flow rate for water or for fluids with similar viscosity values, relative to water. To measure the mass flow rate of the polyacrylamide solutions, an Adam PGL 2002 scale is used. The fluid mass flow rate is determined by collecting the fluid exiting the pump on the scale and recording the change in mass of fluid over a specified time interval.

Polyacrylamide Polymer Solutions

The polymer fluid mixture which is utilized in this present study has a viscosity value from 0.0175 to 0.0231 Pa·s at 20 °C (where different values are associated with different shear rates). A concentration of 3000 ppm of PAAm polymer is employed, with 1% NaCl and 3% isopropanol. The procedure for mixing the stock solution is adopted from Groisman and Steinberg [12]. To mix a 3000 ppm solution, 3 g of NaCl is dissolved in 275 mL DI water by a commercial mixer. After all the NaCl is dissolved, 0.9 g of PAAm (Polyacrylamide, Mw = 18,000,000 Da, Polysciences Inc., Warrington, PA) powder is gently mixed for 3 h in a commercial mixer with propeller at moderate speed. This is done to degrade the polymer slightly, so it does not degrade significantly during tests. After the timed 3 h, 9 g of isopropanol is added and mixed into the solution. Finally, DI water is added to bring the total mass of the solution to 300 g depending on the desired fluid viscosity.

In testing with both the rheometer and disk pump, no effects due to additional degradation are evidenced by the repeatability of measured data. Such repeatability is established from measurements of pressure rise at particular values of volumetric flow rate and disk rotational speed. Note that such measurements are conducted in a steady fashion as a polymer solution is advected continuously through the VDP. Initial loading of the polymer solution occurs as each solution is first advected into the inlet of the VDP flow passage. Because each polymer solution is present within the VDP over a finite time period, the present flow arrangement imposes stresses upon the flow field in a temporary manner during the time that the polymer solutions are present within the VDP flow passage. With this arrangement, shear rates are generally somewhat higher than in previous investigations [12].

Polymer mixture rheological data are obtained using a state-of-the-art commercial Anton Paar Rheometer MCR 302. These data are employed to provide information regarding viscosity properties, as dependent upon shear rate and polymer concentration. Such data are determined through a power-law shear stress–shear rate relationship. Table 1 presents a summary of the rheological properties of the polyacrylamide solution utilized within the present investigation.

Experimental Uncertainty Estimates

A first-order uncertainty analysis is performed using a constant-odds combination method, based on a 95% confidence level as described by Moffat [13]. The flow passage height variation across the fluid chamber is less than 1.5 μm, with a measured variation less than 1.1 μm ($\pm 0.55\ \mu$m) for $h = 230\ \mu$m, which is 0.55% of h. The value 0.55% is the maximum percent variation of flow passage height for the flow passage height tested. The

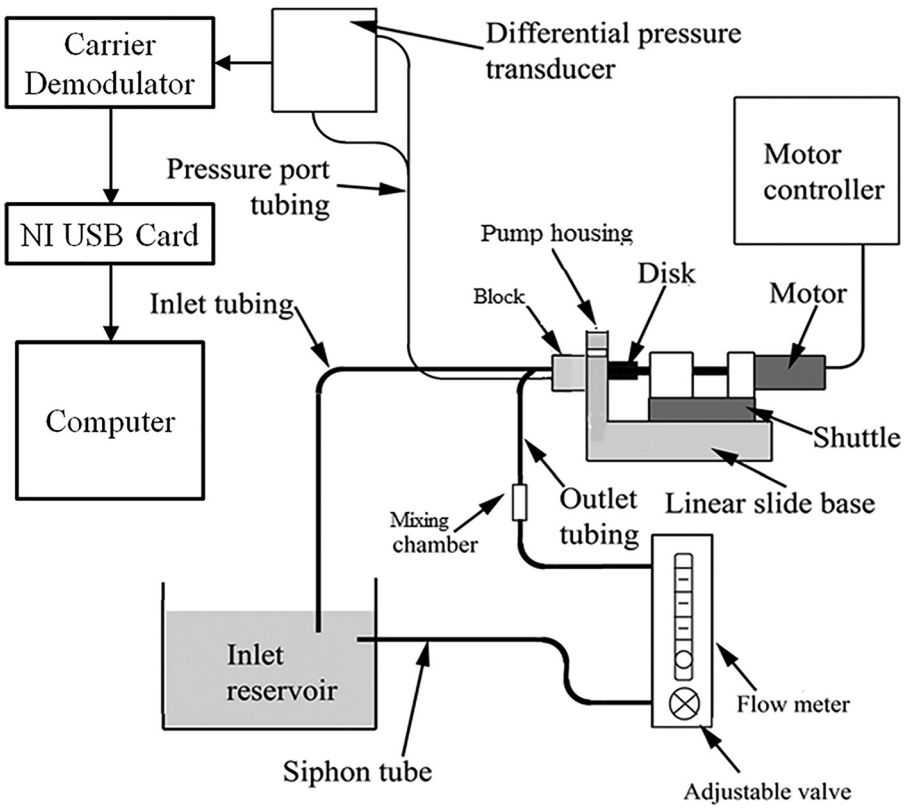

Fig. 3 Arrangement and components for the single-disk viscous pump for pressure measurements. All the dimensions are given in millimeters.

Downloaded From: http://fluidsengineering.asmedigitalcollection.asme.org/pdfaccess.ashx?url=/data/journals/jfega4/935857/ on 03/31/2017 Terms of Use: http://www.asme.org/a

Table 1 Rheological and flow properties of the polyacrylamide solutions for the present investigation, with 3000 ppm PAAm, 1% NaCl, and 3% isopropanol at a temperature of 20 °C

Rotation rate (1/s)	VDP shear rate (1/s)	Rheometer shear rate (1/s)	μ (Pa·s)	Re	Substance
126	975.1	275	0.0175	2.9	Polyacrylamide solution
188	1455.0	400	0.0193	4.0	Polyacrylamide solution
262	2027.7	600	0.0214	5.0	Polyacrylamide solution
366	2832.5	800	0.0231	6.5	Polyacrylamide solution
126	975.1	—	0.001	51.6	Pure water solution
188	1455.0	—	0.001	77.0	Pure water solution
262	2027.7	—	0.001	107.3	Pure water solution
366	2832.5	—	0.001	149.8	Pure water solution

Fluid type	n	K (Pa·s^n)	ρ (kg/m^3)
3000 ppm polyacrylamide	1.2608	0.002978	1000
Water	1	0.001	1000

resulting uncertainty magnitudes associated with experimentally measured pressure rise, flow passage height, fluid viscosity, disk rotational speed, pump chamber radii, and flow rate are presented in Table 2.

Flow Analysis for the Miniature Viscous Disk Pump

Ligrani et al. [9,11] provided relationships between volumetric flow rate and pressure rise for the viscous disk pump. ΔP is denoted as the pressure rise over the circumferential angle $\Delta\theta$, between the two pressure ports $(p_2 - p_1)$ shown in Fig. 2. $\Delta\theta$ is then the angle between the pressure ports and is equal to $\pi/2$. The volumetric flow rate is determined from the integral of the circumferential velocity v_θ with respect to the cross-sectional area of the viscous disk pump. According to the analyses presented in these investigations [9,11], because the flow passage height h is small, $h/(R_2 - R_1) \ll 1$, and changes of local circumferential velocity v_θ across the z-direction over the distance h are much larger than the changes of v_θ in the r-direction over the distance $R_2 - R_1$. As a result, the only significant advection or diffusion term of the partial differential equation for conservation of v_θ momentum is the one representing diffusion of v_θ in the z-direction. In addition, the shear rate for the flow is given by dv_θ/dz, which is equal to V/h for the mean radial circumference of the VDP, provided contributions from the pressure gradient are neglected. According to Ligrani et al. [9,11], the resulting dimensional volumetric flow rate is then given by

$$Q = \frac{\omega h(R_2^2 - R_1^2)}{4} - \frac{h^3(R_2 - R_1)\,\Delta P}{6\mu(R_1 + R_2)\,\Delta\theta} \tag{1}$$

This equation gives results which are numerically equivalent to an equation from Blanchard et al. [10]. Note that different forms of these two equations are a result of different z-coordinate origin locations.

Results and Discussion

The experimentally measured data illustrate pressure rise and flow rate characteristics of the viscous disk pump. Of particular interest are flow behavior deviations from nominal Newtonian behavior, due to the presence of non-Newtonian elastic turbulence. All the data are given for a flow passage height h of 230 μm. Disk dimensional rotational speeds of 1200 rpm, 1800 rpm, 2500 rpm, and 3500 rpm are employed, which are equivalent to respective rotational speeds of 126 1/s, 188 1/s, 262 1/s, and 366 1/s.

Viscosity Variations for Non-Newtonian Polyacrylamide

In general, determination of relationships between shear stress and shear rate and between viscosity and shear rate is challenging for viscoelastic polymer solutions [12,14]. This is because of the inherent memory effects of such solutions, which generally appear as significant hysteresis, which occurs as viscosity, shear stress, and shear rate relationships change, depending on whether or not the fluid solution is undergoing loading (with shear rate increasing) or undergoing unloading (with shear rate decreasing). As a result, the rate of polymer stretching (from the shear rate) is important, and associated properties may vary with time, depending upon the test configuration. In addition, if loading of a viscoelastic polymer solution is followed by unloading, permanent deformation may develop.

Within the present experiment, initial loading of the polymer solution occurs as it is first advected into the inlet of the VDP flow passage. Afterward, the loading and imposed spatially averaged shear rate are continuous and steady, as the polymer solution is present within the VDP flow passage, and as the polymer solution is advected continuously through the VDP. As such, the viscosity model for the present arrangement corresponds to this arrangement. Note that the present power-law model is applied only to one polymer solution, and as a result, the model does not account for changing molecular effects, for example, to account for polymers with different molecular weights. Other investigators who have employed viscosity power-law models to non-Newtonian viscoelastic polymer solutions, as well as to Newtonian fluid flows, include Flumerfelt et al. [15], Hashmet et al. [16], and Al-Fariss and Al-Zahrani [17].

Such power-law models offer an approach to determine effective absolute viscosity values and associated relationships between shear stress and shear rate. With the appropriate experimental conditions, such models provide appropriate means to account for the non-Newtonian influences which are associated with polyacrylamide. Analytically, such power-law models are described using an equation given by

$$\tau = \mu_{\text{eff}}\left(\frac{dv_\theta}{dz}\right) = K\left|\frac{dv_\theta}{dz}\right|^{n-1}\left(\frac{dv_\theta}{dz}\right) \tag{2}$$

Here, K is the flow consistency index, a constant, and n is the dimensionless flow behavior index. Figure 4 presents

Table 2 Experimental uncertainties associated with experimental data

Variable	Maximum percent uncertainty (%)
ΔP	5.00
Q	2.50
H	2.75
M	2.00
Ω	1.50
R_1,R_2	1.10

Downloaded From: http://fluidsengineering.asmedigitalcollection.asme.org/pdfaccess.ashx?url=/data/journals/jfega4/935857/ on 03/31/2017 Terms of Use: http://www.asme.org/a

experimental strain rate and shear stress data obtained using the Anton Paar Rheometer MCR 302 for the polyacrylamide solution which employed within the present study. These experimental data show agreement with results obtained using Eq. (2) with n and K values of 1.261 and 0.00298, respectively. Note that different rotational speeds along the horizontal axis of Fig. 4 correspond to different shear rate values.

Dimensional Pressure Rise Variations With Dimensional Volumetric Flow Rate for Different Disk Rotational Speeds

Variations of dimensional pressure rise with dimensional volumetric flow rate are illustrated by the data given in Figs. 5 and 6, where each data set is obtained at constant disk rotational speed. The experimental data within Fig. 5 are obtained only using pure water as the working fluid. The experimental data within Fig. 6 are obtained using pure water and with the polyacrylamide solution as the working fluids, with rotational speeds (ω) between 126 1/s and 366 1/s. Flow passage height is 230 μm for the data in both figures. As the disk rotational speed is held constant, the flow rate is varied by changing the adjustable valve on the flow meter which is shown in Fig. 3.

The solid lines in Fig. 5 represent analytically determined values using Eq. (1) for a pure Newtonian water for disk rotational speeds of 126 1/s, 188 1/s, 262 1/s, and 366 1/s. Associated pure water experimental data are also included within the figure. These results generally show a linear relationship between the dimensional pressure rise and dimensional flow rate for the VDP for each different impeller rotational speeds, which is consistent with results from a variety of other macroscale pumps [2,4]. For all the four values of ω, pressure rise increases as flow rate decreases, such that maximum pressure rise is present for $Q = 0$, and the maximum flow rate is present for $\Delta P = 0$. Figure 5 also shows that the experimental data are in reasonable agreement with Eq. (1). Note that the slopes of the data for each rotational speed in Fig. 5 are approximately the same as volumetric flow rate varies, for each value of disk rotational speed.

The dimensional pressure rise and dimensional volumetric flow rate experimental data in Fig. 6 are given for pure water and for the polyacrylamide solution flow, for disk rotational speeds of 126 1/s, 262 1/s, and 366 1/s. Here, the pure water data in Fig. 6 are the same data which are presented in Fig. 5. In regard to the polyacrylamide data in Fig. 6, overall, qualitative trends show some similarity to results in Fig. 5, in that pressure variation data show negative slopes for each disk rotational speed. However, in contrast to the data in Fig. 5, the slopes of the polyacrylamide

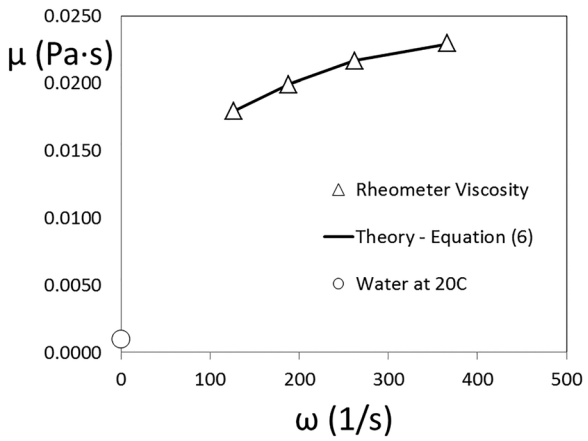

Fig. 4 Dimensional absolute viscosity variation with dimensional disk rotational speed, from the Anton Paar Rheometer MCR 302, and determined using effective viscosity values from Eq. (2)

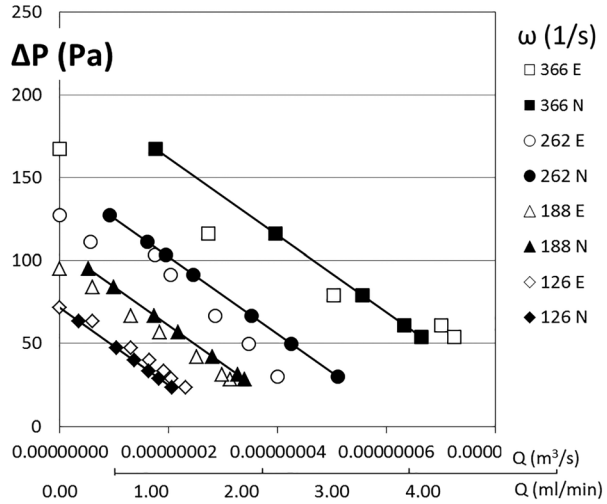

Fig. 5 Dimensional pressure rise variation with dimensional volumetric flow rate for pure water for disk rotational speeds from 126 1/s to 366 1/s. The chamber height of the single-disk viscous pump is 230 μm. *N* is the Newtonian fluid analytic result, and *E* is the experimental data. Note that the lines and solid symbols (denoted with *N*) provide analytically predicted results.

pressure rise data in Fig. 6 vary with volumetric flow rate and with disk rotational speed. The polyacrylamide pressure rise data in this figure are also substantially higher than the pure water data, when compared at the same disk rotational speed ω and dimensional volumetric flow rate Q. Such slope variations and increased pressure rise values evidence different levels of non-Newtonian elastic turbulence behavior, and different levels of mixing associated with different magnitudes of polymer agitation.

Larger elastic turbulence deviation from pure water Newtonian behavior is expected as local fluid shear stress levels increase. Within the present VDP, such increases are associated with larger pressure increases, and smaller volumetric flow rates, for a particular value of ω. When compared at particular values of volumetric flow rate Q and dimensional disk rotational speed ω, lower elastic

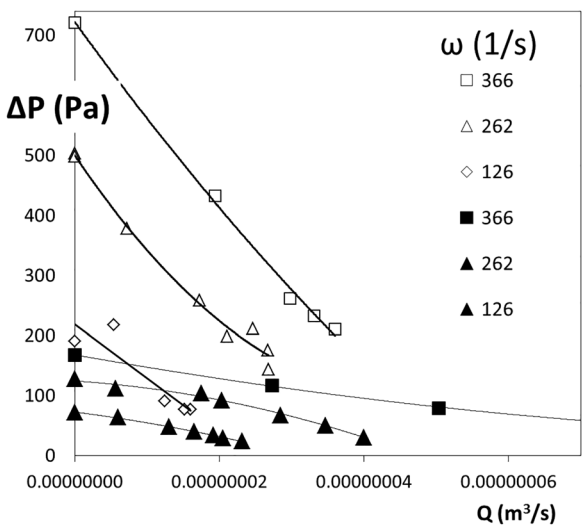

Fig. 6 Dimensional pressure rise variation with dimensional volumetric flow rate for the single-disk viscous pump for disk rotational speeds of 126 1/s, 262 1/s, and 366 1/s. The pump chamber height is 230 μm. Data are given for a pure water solution (closed symbols), and for a polyacrylamide solution (open symbols). Note that lines are included within the figure to show data trends.

Downloaded From: http://fluidsengineering.asmedigitalcollection.asme.org/pdfaccess.ashx?url=/data/journals/jfega4/935857/ on 03/31/2017 Terms of Use: http://www.asme.org/a

turbulence pressure rise values, relative to pure water Newtonian data in Fig. 6 means that local stress magnitudes are also lower. Such behavior is a result of increased mixing and increased transport, which occur as elastic turbulence effects become more pronounced. As a result, differences between the two types of flow behavior are much more significant when the dimensional disk rotational speed ω is 366 1/s, relative to results obtained at lower disk rotational speeds. Transport, mixing, and pressure rise are augmented by elastic turbulence as polymers are stretched in constriction by flow strain, which is induced by streamline curvature within the present VDP. The mechanical stresses act on the polymers within the flow stretching the polymers, causing a secondary flow. This secondary flow acts back on the polymers within the solution and stretches them further causing increased mixing and chaotic fluid motions. In many situations, such activity results in intertwining of different polymer chains within the flow. As a result, the VDP flow transitions from laminar to turbulent flow through elasticity (rather than inertia) at very low Reynolds numbers [12].

Reynolds number for the VDP passage is defined using an equation given by

$$\mathrm{Re} = \frac{\rho\omega(R_2 + R_1)h}{2\mu} \tag{3}$$

With the polyacrylamide solution flows, the Reynolds number with a flow passage height of 230 μm ranges from 2.9 to 6.5 for rotational speeds from 126 1/s to 366 1/s. With pure water flows, the Reynolds number with a flow passage height of 230 μm ranges from 51.6 to 149.8 for rotational speeds from 126 1/s to 366 1/s. Additional details are provided in Table 1. One assumption made in deriving the analytic result given by Eq. (1) is that the Reynolds number is small. This range of Reynolds number validity allows neglecting advection terms in associated flow momentum equations [9,11]. However, note that some of these advection terms are also negligible because the flow in the passage is maintained at or near to a fully developed flow condition [9,11].

Dimensional Pressure Rise Variations With Disk Rotational Speed for Fixed Volumetric Flow Rate

Considered here are maximum dimensional pressure rise variations with dimensional disk rotational speed, for a pump operating condition wherein the overall volumetric flow rate is zero ($Q = 0$). Also considered are the dimensional pressure rise variations with dimensional disk rotational speed, for a pump operating condition, wherein the overall volumetric flow rate is maintained constant at approximately 0.00000002 m^3/s. These particular data are given in Figs. 7 and 8 for pure water and for the polyacrylamide solution flows, for disk rotational speeds of 126 1/s, 188 1/s, 262 1/s, and 366 1/s.

Comparisons of the results in Figs. 7 and 8 show that somewhat lower values are present at each disk rotational speed when the volumetric flow rate Q is maintained constant at approximately 0.00000002 m^3/s, relative to results for $Q = 0$ m^3/s. These two figures also show that pump pressure rise varies linearly with rotational speed for all the four data sets associated with pure water flow. Such behavior is consistent with Eq. (1). In contrast to these Newtonian results, pressure rise data for the polyacrylamide solution flows in Figs. 7 and 8 show more complex variations as disk rotational speed changes. Such trends are consistent with the polyacrylamide solution viscosity increases in Fig. 4, and the complex nonlinear stress strain variations, greater polymer agitation, and increased mixing which are associated with non-Newtonian elastic turbulence.

Head Coefficient and Dimensional Power Variations With Flow Coefficient

Figure 9 shows HC variation with flow coefficient (FC) for disk rotational speeds of 126 1/s, 188 1/s, 262 1/s, and 366 1/s. Figures 9(*a*) and 9(*b*) show results for the pure water solution and the polyacrylamide solution, respectively. Within Fig. 9(*a*), HC decreases continually as disk rotational speed ω increases for the pure water flow, for each value of flow coefficient (FC). Such behavior is consistent with ordinary macroscale fluid pumps [2,4]. In contrast, HC for the polyacrylamide solution flow in Fig. 9(*b*) is approximately the same for ω values of 188 1/s and 126 1/s. As ω increases further, head coefficient values decrease in a significant fashion for each flow coefficient value. Also important are the significantly higher HC values for the polyacrylamide solution flow, compared to the pure water flow, when compared at the same values of flow coefficient and disk rotational speed.

The dimensional power data in Fig. 10 also show different behavior between the pure water flows and the polyacrylamide solution flows. Here, dimensional power Pr is given as microwatts (μW) and is equal to $Q \times \Delta P$. For each fluid type, dimensional power generally increases continually as disk rotational speed ω increases, when compared at the same value of flow coefficient. Values for the polyacrylamide solution flow are then generally higher than the pure water flow values, provided values are compared at the same flow coefficient and disk rotational speed. Other important differences are in relation to maximum power values for a particular disk rotational speed. These occur at optimal Q and ΔP values, which are present as a result of decreasing ΔP with FC, which occurs as Q is increasing with FC. For a disk rotational speed ω of 366 1/s, power maximum occurs for a FC of approximately 0.32 for the pure water flow, and for a flow coefficient of approximately 0.1 for the polyacrylamide solution flow.

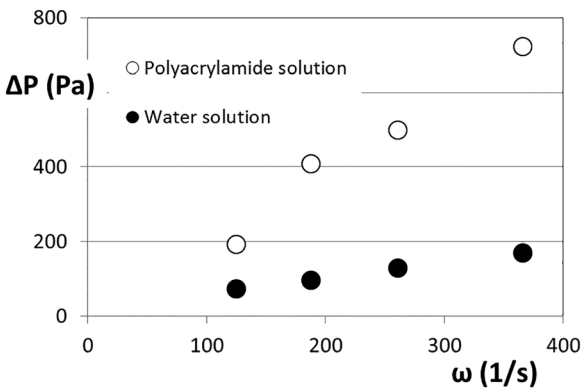

Fig. 7 Dimensional pressure rise variation with dimensional disk rotational speed for the pure water and for the polyacrylamide solution with zero volumetric flow rate, $Q = 0$. The viscous disk pump chamber height is 230 μm.

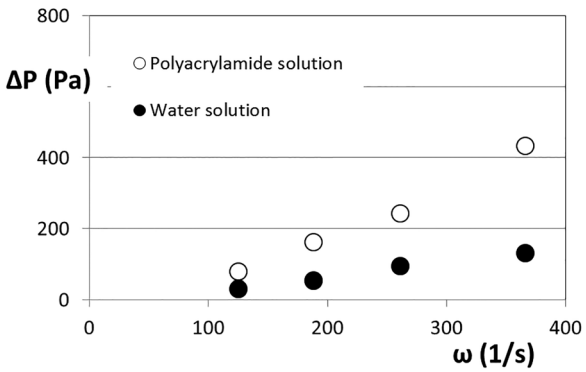

Fig. 8 Dimensional pressure rise variation with dimensional disk rotational speed for the pure water and for the polyacrylamide solution with a volumetric flow rate Q of 0.00000002 m^3/s. The viscous disk pump chamber height is 230 μm.

Downloaded From: http://fluidsengineering.asmedigitalcollection.asme.org/pdfaccess.ashx?url=/data/journals/jfega4/935857/ on 03/31/2017 Terms of Use: http://www.asme.org/a

Such differences evidence significantly different flow and pressure rise characteristics for the two different fluid solutions.

Pump Slip Coefficient

Pump slip coefficient or slip factor is ordinarily determined for local circumferential velocities at the exit of an impeller. The local coefficient value is then the ratio of actual local circumferential velocity to the ideal, local circumferential velocity, where the flow trajectory is determined by the contour of impeller blades without slippage [18,19].

Within the present investigation, determination of such local circumferential velocities is not possible. Instead, overall, average slip coefficients are determined. As such, $\overline{v_\theta}$, the circumferential velocity, spatially averaged for the flow cross-sectional area, is determined using an equation given by

$$\overline{v_\theta} = Q/[h(R_2 - R_1)] \tag{4}$$

The ideal circumferential velocity without slippage, averaged for the flow cross-sectional area, is then given by $\overline{v_{\theta\text{ideal}}}$. This quantity is determined as the disk-induced velocity, without slip for pure Couette flow, for the midradius and midheight location of the VDP channel. The ideal velocity is then given by an equation of the form

$$\overline{v_{\theta\text{ideal}}} = \omega[(R_1 + R_2)/4] \tag{5}$$

The overall slip coefficient (SC) is then given by

$$\text{SC} = \overline{v_\theta}/\overline{v_{\theta\text{ideal}}} \tag{6}$$

With this form, the slip coefficient (SC) then provides a quantitative measure of the ability of the VDP to produce flow which follows the rotating disk, relative to an ideal arrangement with no slip. The parameter ranges between 0 and 1, with more idealized behavior characterized by higher SC values.

Figure 11 presents the slip coefficients, determined using Eq. (6), as they vary with head coefficient for the single-disk viscous pump for disk rotational speeds of 126 1/s, 188 1/s, 262 1/s, and 366 1/s. Here, data are given for pure water (closed symbols), and for polyacrylamide solutions (open symbols). The polyacrylamide solution data cover a wider range of HC, with values as high as 3.8, whereas the water solution data extend to HC values up to about 1.5. Slip coefficients are as high as approximately 0.55 for the polyacrylamide solutions, and as high as about 0.8 for the water. Note that these SC variations are in part a consequence of the natural variation of HC with volumetric flow rate. As a result, slip coefficients decrease to zero values as HC increases for each value of disk rotational speed ω.

The lower range of SC values in Fig. 11 for the polyacrylamide solution data, compared to the pure water data, is believed to be due to larger second law losses when elastic turbulence is present. Such losses are connected to higher viscosity values (Fig. 4) as well as to larger magnitudes of flow slip, for certain values of HC. Increased elastic turbulence loss magnitudes occur as the elastic polymers are excited by mechanical stress, which causes them to extend, become deformed, and become stretched. Such polymer alterations lead to increased magnitudes of local elastic stress. As such, the presently observed loss increases with increased

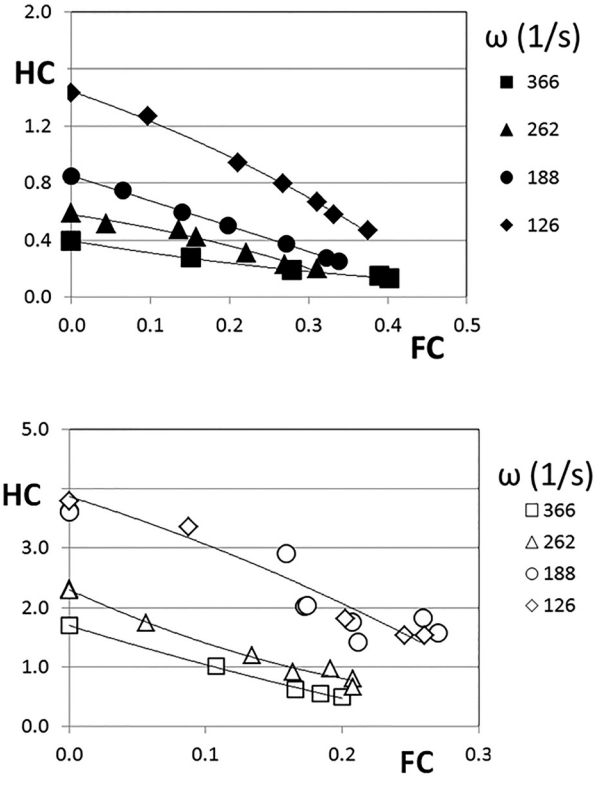

Fig. 9 Head coefficient variation with flow coefficient for the single-disk viscous pump for disk rotational speeds of 126 1/s, 188 1/s, 262 1/s, and 366 1/s. The pump chamber height is 230 μm. (*a*) Pure water solution and (*b*) polyacrylamide solution. Note that lines are included within the figure to show data trends. Also note that only one line is employed within the lower figure to show data trends for rotational speeds of 126 1/s and 188 1/s.

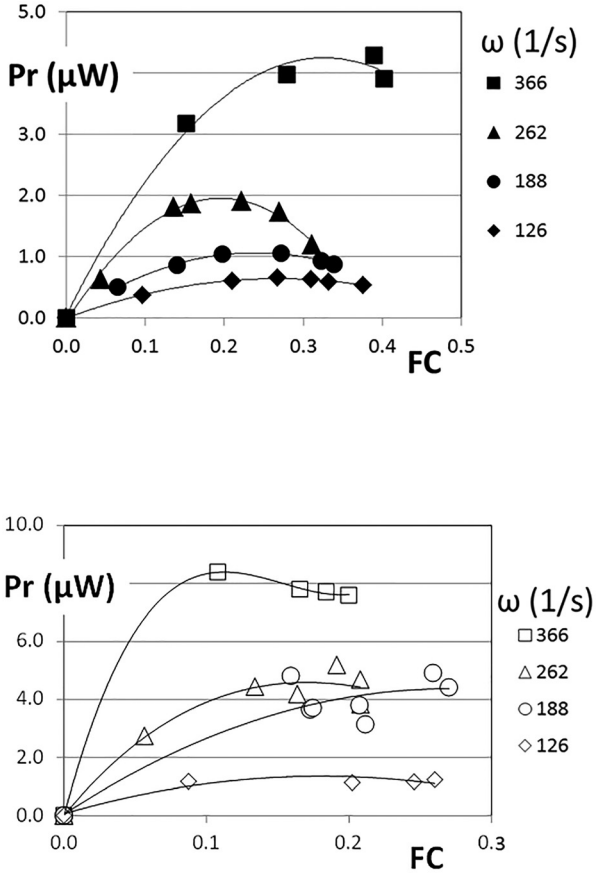

Fig. 10 Dimensional power variation with flow coefficient for the single-disk viscous pump for disk rotational speeds of 126 1/s, 188 1/s, 262 1/s, and 366 1/s. The pump chamber height is 230 μm. (*a*) Pure water solution and (*b*) polyacrylamide solution. Note that lines are included within the figure to show data trends.

Downloaded From: http://fluidsengineering.asmedigitalcollection.asme.org/pdfaccess.ashx?url=/data/journals/jfega4/935857/ on 03/31/2017 Terms of Use: http://www.asme.org/a

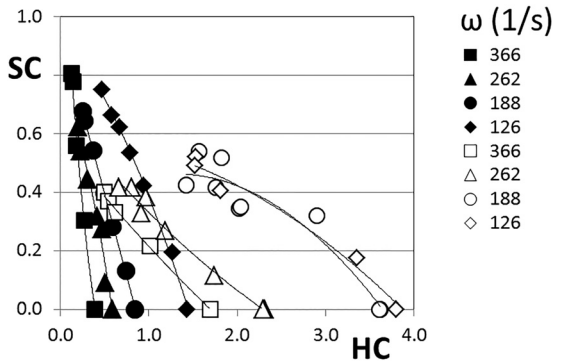

Fig. 11 Slip coefficient variation with head coefficient for the single-disk viscous pump for disk rotational speeds of 126 1/s, 188 1/s, 262 1/s, and 366 1/s. The pump chamber height is 230 μm. Data are given for pure water solutions (closed symbols), and for polyacrylamide solutions (open symbols). Note that lines are included within the figure to show data trends.

viscosity are qualitatively consistent with the results for macroscale fluid pumps which are described by Li [2] and Zhang et al. [3].

Characterization of Elastic Turbulence Fluid Behavior Within the Viscous Disk Pump

To characterize elastic turbulence effects within the VDP, several different parameters are considered. The first of these is ΔP^*, as this quantity changes with dimensional volumetric flow rate and disk rotational speed. Here, ΔP^* is the dimensional pressure rise change at a particular flow rate and disk rotational speed, as the flow changes from pure water Newtonian behavior to elastic turbulence behavior. These data are obtained from the results which are presented in Fig. 6. Figure 12 shows that ΔP^* becomes more pronounced as the volumetric flow rate decreases, and as the disk dimensional rotational speed increases. In most cases, the variation of ΔP^* with dimensional volumetric flow rate is nonlinear, for each disk rotational speed.

Figure 13 shows HCR, the ratio of head coefficient for the polyacrylamide solution and head coefficient for the water solution, as it varies with flow coefficient for the single-disk viscous pump for disk rotational speeds of 126 1/s, 262 1/s, and 366 1/s. These data collect into a single grouping for all the three disk rotational speeds for FC values which are greater than 0. When FC = 0, HCR values range from 2.7 to 4.3, and increase in value as disk rotational speed ω increases. An even better data collapse is

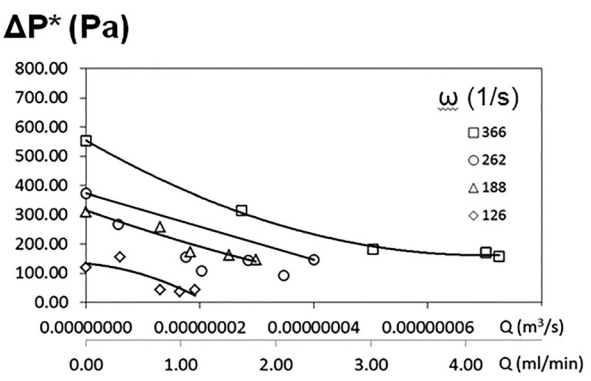

Fig. 12 Dimensional pressure difference (ΔP^*) (between pure water flow and polyacrylamide solution flow) variation with dimensional volumetric flow rate. Data are given for disk rotational speeds of 366 1/s, 262 1/s, 188 1/s, and 126 1/s. The viscous disk pump chamber height is 230 μm. Note that lines are included within the figure to show data trends.

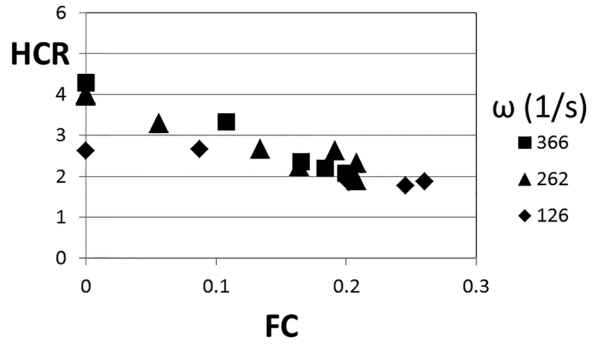

Fig. 13 Ratio of head coefficient for the polyacrylamide solution and head coefficient for the water solution, as it varies with flow coefficient for the single-disk viscous pump for disk rotational speeds of 126 1/s, 262 1/s, and 366 1/s. The pump chamber height is 230 μm.

provided by the PrR data which are given in Fig. 14. Here, PrR is the ratio of pump power for the polyacrylamide solution and pump power for the water solution, as it varies with flow coefficient. These data are also provided for disk rotational speeds of 126 1/s, 262 1/s, and 366 1/s, and a pump chamber height of 230 μm. An important feature of these data is the maximum PrR value which is present for a flow coefficient value of approximately 0.1. As such, the PrR and HCR parameters characterize the performance of the viscous disk pump, relative to Newtonian water flow, for flow coefficients from 0 to 0.3 and for disk rotational speeds from 126 1/s to 366 1/s.

Viscous Disk Pump-Specific Speed

Specific speed data as they vary with flow coefficient are presented in Fig. 15. These results are given for disk rotational speeds of 126 1/s, 188 1/s, 262 1/s, and 366 1/s for the pure water solution and the polyacrylamide solution. Here, pump-specific speed (SS) is given by an equation of the form

$$SS = [\omega(Q)^{1/2}]/(gH)^{3/4} = [\omega(Q)^{1/2}]/(\Delta P/\rho)^{3/4} \quad (7)$$

This form of specific speed is nondimensional, and as such, is determined using volumetric flow rate Q given as m^3/s, acceleration due to gravity g given as m/s^2, pump head H given as meters, and rotational speed ω given using radians per second [20].

The specific speed data for pure water in Fig. 15(*a*) range from 0 to 0.9 for flow coefficients ranging from 0.0 to 0.4. In contrast, specific speed data for the polyacrylamide solution in Fig. 15(*b*)

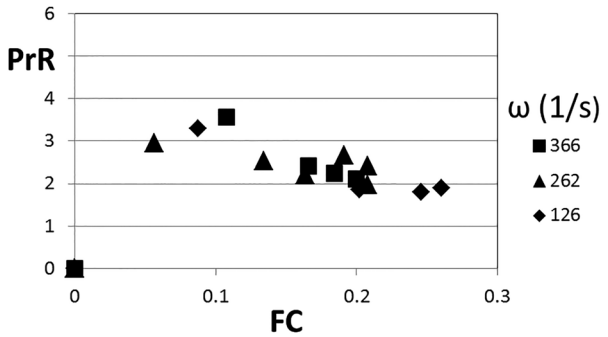

Fig. 14 Ratio of pump power for the polyacrylamide solution and pump power for the water solution, as it varies with flow coefficient for the single-disk viscous pump for disk rotational speeds of 126 1/s, 262 1/s, and 366 1/s. The pump chamber height is 230 μm.

Downloaded From: http://fluidsengineering.asmedigitalcollection.asme.org/pdfaccess.ashx?url=/data/journals/jfega4/935857/ on 03/31/2017 Terms of Use: http://www.asme.org/a

range from 0 to 0.23 for flow coefficients ranging from 0.0 to 0.28. Such specific speeds generally apply to different configurations of fluid pumps, including centrifugal flow, mixed flow, and axial flow devices [20]. The present VDP arrangement is significantly different from these configurations. Nonetheless, different ranges of specific speed for the pure water and polyacrylamide solutions evidence different flow characteristics within the VDP passage, especially in regard to the ability of the fluids to follow the motion of the rotating disk with or without varying amounts of slip.

For example, higher values of specific speed for the pure water arrangement in Fig. 15(*a*) are associated with flow which, in an ordinary fluid pump, is more axial. Within the present VDP, this is believed to further evidence flow which follows the motion of the rotating disk more closely, compared to situations when specific speed values are lower. Such behavior is thus associated with less slippage, and higher values of SC, which is consistent with the results which are presented in Fig. 11. Lower values of specific speed for the polyacrylamide arrangement are associated with flow which, in an ordinary fluid pump, is more centrifugal. The lower range of specific speed for the polyacrylamide solution flow in Fig. 15(*b*) is thus associated with greater slippage, larger second law losses, and generally lower slip coefficient values, even though overall dimensional pressure rise values and HC values are significantly higher, when compared at the same dimensional volumetric flow rate, same FC, and same disk rotational speed ω.

Another important difference between the performance of the VDP with pure water flow and with the polyacrylamide solution is related to variations with disk rotational speed ω. Within Fig. 15(*a*), SS for the pure water flow increases continually with disk rotational speed ω, for a particular value of FC. Such behavior is consistent with that of an ordinary macroscale fluid pump. In contrast, SS for the polyacrylamide solution flow in Fig. 15(*b*) is approximately the same for ω values of 188 1/s and 126 1/s. As ω increases further, specific speed values increase dramatically for each value of flow coefficient. Such complicated trends are due to nonlinear, non-Newtonian elastic turbulence effects, especially the complex interactions which develop as strain is applied to the flow and intricate polymer intertwining and tangling ensue.

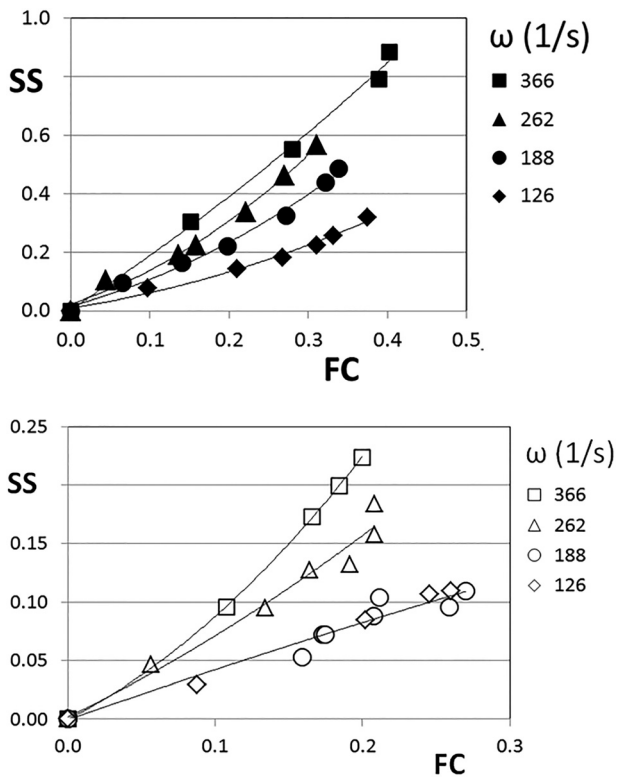

Fig. 15 Specific speed variation with FC for the single-disk viscous pump for disk rotational speeds of 126 1/s, 188 1/s, 262 1/s, and 366 1/s. The pump chamber height is 230 μm. (*a*) Pure water solution and (*b*) polyacrylamide solution. Note that lines are included within the figure to show data trends.

Summary and Conclusions

Within the present investigation, a miniature VDP of millimeter-scale, with a channel depth of 230 μm, is utilized as the behavior and performance are altered by elastic turbulence. The present experimental data are given for rotational speeds of 126 1/s, 188 1/s, 262 1/s, and 366 1/s, pressure rises as high as 700 Pa, and flow rates up to approximately 0.00000005 m^3/s. The non-Newtonian effects of elastic turbulence are induced by adding a specified concentration of polymers (polyacrylamide) to purified water along with NaCl to ionize the polymer components and are considered relative to Newtonian behavior. The VDP is utilized because it produces easily controlled flow rates and pressure rises, as simplicity and ease of manufacturing are maintained [9,11]. The disk pump is also unique because it uses viscous stress to produce a pumping effect by employing one disk and a C-shaped channel [9,11]. As the fluid passage height becomes smaller, the Reynolds number decreases, and the viscous forces become more significant relative to inertial forces. For rotational speeds from 126 1/s to 366 1/s, Reynolds number ranges from 2.9 to 6.5 for the non-Newtonian polyacrylamide solution flows, and from 51.6 to 149.8 for the Newtonian pure water flows.

To characterize deviations due to non-Newtonian elastic turbulence phenomena, two new parameters are introduced, PrR and HCR. Here, HCR is the ratio of head coefficient for the polyacrylamide solution and head coefficient for the water solution, and PrR is the ratio of pump power for the polyacrylamide solution and pump power for the water solution. As FC, the flow coefficient ranges from 0 to 0.3, for disk rotational speeds from 126 1/s to 366 1/s, HCR and PrR values both collect into single groupings, provided FC values are greater than zero.

In contrast to Newtonian, pure water data, the slopes of the polyacrylamide pressure rise data vary with volumetric flow rate and with disk rotational speed. The polyacrylamide pressure rise data are also substantially higher than the pure water data, when compared at the same disk rotational speed ω and dimensional volumetric flow rate Q. Such slope variations and increased pressure rise values evidence different levels of non-Newtonian elastic turbulence behavior, with larger elastic turbulence deviations from pure water Newtonian behavior as local fluid shear stress levels increase. Within the present VDP, such increases are associated with larger pressure increases, and smaller volumetric flow rates, for a particular value of rotational speed ω.

These pressure rise data are also considered in nondimensional form in terms of the HC or head coefficient. In general, head coefficient values *decrease in a significant fashion* as rotational speed ω increases, for each FC value, for both water and polyacrylamide flow solutions. In contrast, dimensional power generally *increases continually* as disk rotational speed ω increases, when compared at the same value of FC, for both water and polyacrylamide flow solutions. Both HC and dimensional power, for the polyacrylamide solution flows, are significantly higher than pure water flow values, when compared at the same values of flow coefficient and disk rotational speed. Other important differences are in relation to maximum power values for a particular disk rotational speed. For example, for a disk rotational speed ω of 366 1/s, power maximum occurs for a FC of approximately 0.32 for the pure water flow, and for a flow coefficient of approximately 0.1 for the polyacrylamide solution flow.

Different ranges of SS for the pure water and polyacrylamide solutions also evidence different flow characteristics within the

Downloaded From: http://fluidsengineering.asmedigitalcollection.asme.org/pdfaccess.ashx?url=/data/journals/jfega4/935857/ on 03/31/2017 Terms of Use: http://www.asme.org/a

VDP passage, especially in regard to the ability of the fluids to follow the motion of the rotating disk with or without varying amounts of slip. Other SS trends as rotational speed ω varies are due to nonlinear, non-Newtonian elastic turbulence effects, especially the complex interactions which develop as strain is applied to the flow and intricate polymer intertwining and tangling ensue. Such differences are also evidenced by a lower range of SC or slip coefficient values for the polyacrylamide solution flows, compared to the pure water flows. These variations are believed to be due to increased elastic turbulence loss magnitudes, which occur as viscosity magnitudes increase and the elastic polymers are excited by mechanical stress, which causes them to extend, deform, stretch, and intertwine.

Acknowledgment

The research was supported by the U.S. National Science Foundation under Grant No. CBET-1501587. The Anton Paar Corporation is acknowledged for loaning a commercial Anton Paar Rheometer MCR 302 to the University of Alabama in Huntsville for use during the present investigation. Ms. Maria Brown and Ms. Mary Jennerjohn are also acknowledged for their assistance in obtaining some of the experimental data which are presented within the present paper. Note also that the present paper is based, in part, upon the content of our IMECE 2015 conference paper [21].

Nomenclature

(dv_θ/dz) = local fluid shear rate
FC = pump flow coefficient, $Q/[\omega h(R_2 - R_1)\,(R_1 + R_2)/2]$
g = acceleration due to gravity
h = flow passage height of the disk pump
H = pump head, $\Delta P/\rho g$
HC = pump head coefficient, $\Delta P/\rho[\omega(R_1 + R_2)/2]^2$
HCR = ratio of head coefficient with elastic turbulence to head coefficient with purified water, both at the same experimental conditions
k = spring constant
K = flow consistency index
L = characteristic length scale
n = power-law coefficient for non-Newtonian stress–strain relationship
p = local static pressure
Pr = pump power, $Q\,\Delta P$
PrR = ratio of pump power with elastic turbulence to pump power with purified water, both at the same experimental conditions
Q = dimensional volumetric flow rate
r = radial coordinate
R_1 = inner radius of the pump chamber
R_2 = outer radius of the pump chamber
$s = 1/n$
SC = pump slip coefficient
SS = pump-specific speed
v_r = local radial component fluid velocity
v_z = local normal component fluid velocity
v_θ = local circumferential component fluid velocity
$\overline{v_\theta}$ = circumferential component fluid velocity spatially averaged over the flow cross-sectional area
$\overline{v_{\theta\text{ideal}}}$ = ideal circumferential component fluid velocity spatially averaged over the flow cross-sectional area
$V = r\omega$
V_c = characteristic velocity scale
W = channel width
z = normal coordinate
ΔP = dimensional static pressure rise between pressure ports 1 and 2, $p_2 - p_1$
ΔP^* = pressure difference between Newtonian and non-Newtonian elastic turbulence flow at a particular volumetric flow rate and disk rotational speed

Greek Symbols

$\Delta\theta$ = circumferential span between two angular locations
θ = circumferential coordinate
μ = absolute viscosity
μ_{eff} = effective absolute viscosity
ρ = fluid density
τ = local shear stress
ω = rotational speed of the disk, $2\pi\Omega/60$
Ω = dimensional rotational speed of the disk, rpm

References

[1] Yu, S. C. M., Ng, B. T. H., Chan, W. K., and Chua, L. P., 2000, "The Flow Patterns Within the Impeller Passages of a Centrifugal Blood Pump Model," J. Med. Eng. Phys., **22**(6), pp. 381–393.
[2] Li, W.-G., 2000, "Effects of Viscosity of Fluids on Centrifugal Pump Performance and Flow Pattern in the Impeller," Int. J. Heat Fluid Flow, **21**(2), pp. 207–212.
[3] Zhang, G., Zhang, M., Yang, W., Zhu, X., and Hu, Q., 2008, "Effects of Non-Newtonian Fluid on Centrifugal Blood Pump Performance," Int. Commun. Heat Mass Transfer, **35**(5), pp. 613–617.
[4] Memardezfouli, M., and Nourbakhsh, A., 2009, "Experimental Investigation of Slip Factors in Centrifugal Pumps," Exp. Therm. Fluid Sci., **33**(5), pp. 938–945.
[5] da Silva, A. K., Kobayashi, M. H., and Coimbra, C. F. M., 2007, "Optimal Design of Non-Newtonian, Micro-Scale Viscous Pumps for Biomedical Devices," J. Biotechnol. Bioeng., **96**(1), pp. 37–47.
[6] El-Sadi, H., Esmail, N., and Hassan, I., 2008, "Numerical Modeling of Non-Newtonian Flow in Viscous Micropump," J. Soc. Rheol. Jpn., **36** (1), pp. 51–58.
[7] Sen, M., Wajerski, D., and Gad-El-Hak, M., 1996, "A Novel Pump for MEMS Applications," ASME J. Fluids Eng., **118**(3), pp. 624–627.
[8] Berli, C. L. A., 2010, "Output Pressure and Efficiency of Electrokinetic Pumping of Non-Newtonian Fluids," Microfluid Nanofluid J., **8**(2), pp. 197–207.
[9] Ligrani, P. M., Jiang, H., Lund, B., and Jin, J. S., 2013, "Deviations Due to Non-Newtonian Influences Within a Miniature Viscous Disk Pump," ASME J. Fluids Eng., **135**(3), p. 031205.
[10] Blanchard, D., Ligrani, P. M., and Gale, B., 2006, "Miniature Single-Disk Viscous Pump (Single-DVP), Performance Characterization," ASME J. Fluids Eng., **128**(3), pp. 602–610.
[11] Ligrani, P. M., Blanchard, D., and Gale, B., 2010, "Slip Due to Surface Roughness for a Newtonian Liquid in a Viscous Micro-Scale Disk Pump," Phys. Fluids, **22**(5), p. 052002.
[12] Groisman, A., and Steinberg, V., 2000, "Elastic Turbulence in a Polymer Solution Flow," Nature, **405**(6782), pp. 53–55.
[13] Moffat, R. J., 1982, "Contributions to the Theory of Single-Sample Uncertainty Analysis," ASME J. Fluids Eng., **104**(2), pp. 250–260.
[14] Burghelea, T., Segre, E., and Steinberg, V., 2007, "Elastic Turbulence in von Karman Swirling Flow Between Two Disks," Phys. Fluids, **19**(5), p. 053104.
[15] Flumerfelt, R. W., Pierick, M. W., Cooper, S. L., and Bird, R. B., 1969, "Generalized Plane Couette Flow of a Non-Newtonian Fluid," J. Ind. Eng. Chem. Fundamen., **8**(2), pp. 354–357.
[16] Hashmet, M. R., Onur, M., and Tan, I. M., 2014, "Empirical Correlations for Viscosity of Polyacrylamide Solutions With the Effects of Concentration, Molecular Weight, and Degree of Hydrolysis of Polymer," J. Appl. Sci., **14**(10), pp. 1000–1007.
[17] Al-Fariss, T. F., and Al-Zahrani, S. M., 1993, "Rheological Behavior of Some Dilute Polymer Solutions," JKAU: Eng. Sci., **5**(1), pp. 95–109.
[18] Stodola, A., 1945, *Steam and Gas Turbines*, McGraw-Hill Book, New York.
[19] Stanitz, J. D., 1952, "Some Theoretical Aerodynamic Investigations of Impellers in Radial and Mixed Flow Centrifugal Compressors," Trans. ASME, **74**, pp. 473–476.
[20] Sabersky, R. H., Acosta, A. J., and Hauptmann, E. G., 1989, *Fluid Flow: A First Course in Fluid Mechanics*, MacMillan Book, New York.
[21] Lund, B., Brown, M., Jennerjohn, M., Ligrani, P. M., and Fatemi, A., 2015, "Elastic Turbulence Effects on the Performance of a Miniature Viscous Disk Pump," ASME Paper No. IMECE2015-52596.

Downloaded From: http://fluidsengineering.asmedigitalcollection.asme.org/pdfaccess.ashx?url=/data/journals/jfega4/935857/ on 03/31/2017 Terms of Use: http://www.asme.org/a